





Article

# New Insights into Key Determinants for Adenosine 1 Receptor Antagonists Selectivity Using Supervised Molecular Dynamics Simulations

Giovanni Bolcato <sup>1</sup>, Maicol Bissaro <sup>1</sup> , Giuseppe Deganutti <sup>2</sup> , Mattia Sturlese <sup>1</sup>  and Stefano Moro <sup>1,\*</sup> 

<sup>1</sup> Molecular Modeling Section (MMS), Department of Pharmaceutical and Pharmacological Sciences, University of Padova, via Marzolo 5, 35131 Padova, Italy; giovanni.bolcato.1@studenti.unipd.it (G.B.); maicol.bissaro@studenti.unipd.it (M.B.); mattia.sturlese@unipd.it (M.S.)

<sup>2</sup> School of Life Sciences, University of Essex, Wivenhoe Park, Colchester CO4 3SQ, UK; gd17863@essex.ac.uk

\* Correspondence: stefano.moro@unipd.it

Received: 3 April 2020; Accepted: 28 April 2020; Published: 7 May 2020



**Abstract:** Adenosine receptors (ARs), like many other G-protein-coupled receptors (GPCRs), are targets of primary interest in drug design. However, one of the main limits for the development of drugs for this class of GPCRs is the complex selectivity profile usually displayed by ligands. Numerous efforts have been made for clarifying the selectivity of ARs, leading to the development of many ligand-based models. The structure of the AR subtype A<sub>1</sub> (A<sub>1</sub>AR) has been recently solved, providing important structural insights. In the present work, we rationalized the selectivity profile of two selective A<sub>1</sub>AR and A<sub>2A</sub>AR antagonists, investigating their recognition trajectories obtained by Supervised Molecular Dynamics from an unbound state and monitoring the role of the water molecules in the binding site.

**Keywords:** GPCRs; adenosine receptors; selectivity; A<sub>1</sub>AR; A<sub>2A</sub>AR; antagonist; molecular dynamics (MD); supervised molecular dynamics (SuMD)

## 1. Introduction

Adenosine receptors (ARs) are class A G protein-coupled receptors (GPCRs) that bind the endogenous agonist adenosine. ARs are composed of four subtypes: A<sub>1</sub>, A<sub>2A</sub>, A<sub>2B</sub>, A<sub>3</sub>. While A<sub>1</sub> and A<sub>3</sub>ARs (which share 49% of a sequence identity) are preferentially coupled to G<sub>α<sub>i</sub></sub> proteins and therefore inhibit the adenylyl cyclase, A<sub>2A</sub> and A<sub>2B</sub>ARs (sharing 59% of a sequence identity) stimulate this enzyme, as being coupled to G<sub>α<sub>s</sub></sub> proteins [1]. Several ARs antagonists are in clinical trials for various diseases. With regards to A<sub>2A</sub>AR, tradeqylline has been recently approved for Parkinson's disease (NCT02610231) [2], PBF-509 is in phase I/II trials for non-small cell lung cancer (NCT02403193), and CPI-144 is in phase I trials for various cancer types (NCT02655822). PBF-680, on the other hand, is the only A<sub>1</sub>AR antagonist in clinical phase II, for the treatment of Asthma (NCT02635945) [3].

One of the difficulties during the development of ARs agonists and antagonists as therapeutic agents is the poor selectivity between different receptor subtypes [4]. For this reason, many efforts have been made to elucidate the molecular basis of ARs ligands selectivity, and several structure-activity relationship (SAR) models have been developed for selective ligands of all the four subtypes [1,2,5–14].

With the increasing availability of structural information (mainly from mutagenesis, X-ray, and cryo-EM approaches [15]) in the last few years, light has been shed on the origin of selectivity on ARs. Recently, the A<sub>1</sub>AR inactive (PDB, Protein Data Bank, code 5UEN [16] and 5N2S [17]) and active (PDB code 6D9H [18]) structures have been solved. Interestingly, in [17], Cooke and colleagues obtained the X-ray crystal structure of A<sub>1</sub> and A<sub>2A</sub> ARs, in a complex with the same xanthine ligand

PSB36, providing insight about the selectivity. There are several structural differences between  $A_1$ AR and  $A_{2A}$ AR. The second extracellular loop (ECL2), in particular, is more folded in  $A_1$ AR and orients perpendicularly to the plane of the membrane, while in  $A_{2A}$ AR it forms a longer helix, which is parallel to the lipid bilayer. This difference is probably due to the presence of two disulfide bonds uniquely present in  $A_{2A}$ AR. Indeed, the bond between Cys71 and Cys159 anchors ECL2 to ECL1, while the bond between Cys74 and Cys146 tethers TM3 to ECL2. The class A conserved disulfide bond between Cys80 and Cys169 is present in both the two subtypes. These differences in the disulfide bonds likely contribute to the outward movement of the top of transmembrane helix 2 (TM) in the inactive  $A_1$ AR (Figure 1).

Further divergence involves TM7, which is shifted outward compared to  $A_{2A}$ AR, due to the shorter ECL3, and TM6 slightly shifted inward in  $A_1$ AR. These rearrangements, in turn, affect the orthosteric site of  $A_1$ AR, which is wider than  $A_{2A}$ AR. Interestingly, the key residues in the orthosteric site of the two receptors are conserved and drive the same binding mode of the antagonist PSB36 (Figure 1). More precisely, the xanthine scaffold forms two hydrogen bonds with Asn254 ( $A_1$ AR, Asn253 in  $A_{2A}$ AR) and a  $\pi$ - $\pi$  stacking with Phe171 ( $A_1$ AR, Phe168 in  $A_{2A}$ AR). Nevertheless, Asn254 ( $A_1$ AR) is located in the binding site deeper than Asn253 in  $A_{2A}$ AR, and the xanthine ligand is consequently positioned deeply in the orthosteric site (Figure 1).

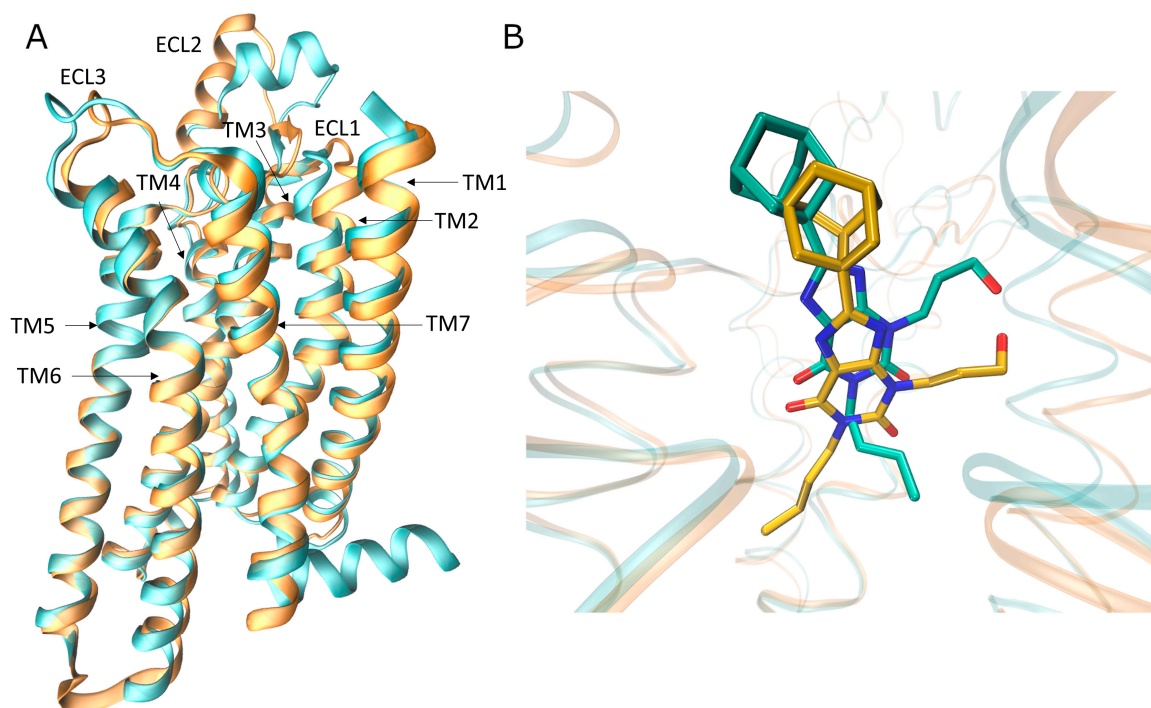


**Figure 1.** Comparison of  $A_1$ AR and  $A_{2A}$ AR structures (A) Superposition of the crystal structure of the inactive  $A_1$  (orange) and  $A_{2A}$  (cyan) adenosine receptors (Ars) (PDB code 5N2S and 5N2R respectively). (B) Superposition of the same xanthine ligand PSB36 in the two aforementioned crystal structures.

Despite the huge help provided from high-resolution structural biology techniques, certain selectivity profiles cannot be only rationalized by the mere coordinates of bound state or “final” state. Ligand recognition is an articulated mechanism in which many variables may play a relevant role and over the last few years, there has been rising attention in the understanding of binding kinetics at GPCRs and its determinant role to successfully target this class of proteins [19].

In the present study, we used supervised molecular dynamics (SuMD) simulations to shed light on the molecular basis of the selectivity of three different ligands to  $A_1$ AR and  $A_{2A}$ AR, not only considering the bound states, but also the possible different recognition mechanism preceding the final orthosteric site and the role of the solvent. We focus our attention on three antagonists: the  $A_{2A}$ AR

selective antagonists Z48 (Ki 16.9 nM in A<sub>2A</sub>AR and 1345.7 nM in A<sub>1</sub>AR) [20]; the A<sub>1</sub>AR selective antagonist LC4 (Ki 16,800 nM in A<sub>2A</sub>AR and 89 nM in A<sub>1</sub>AR) [21]; and the nonselective antagonist caffeine (Figure 2). SuMD [22,23] is a molecular dynamics (MD) approach that allows for the study of molecular recognition processes in a fully atomistic way, in the nanosecond timescale, without introducing any energetic biases.

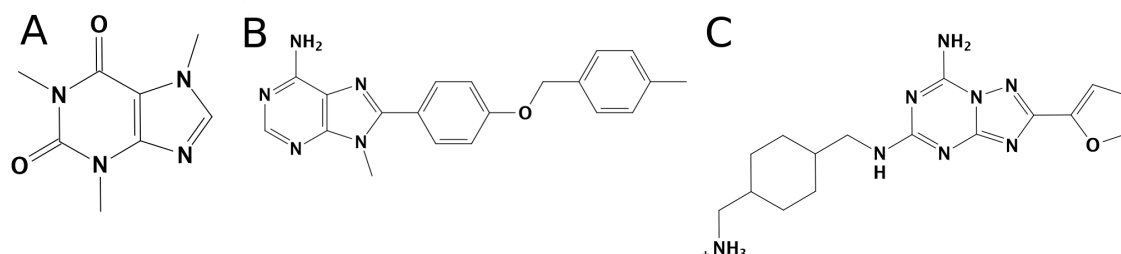


**Figure 2.** The three ligands considered in the present study. (A) Caffeine, a non-selective ARs antagonist. (B) LC4, an A<sub>1</sub>-AR selective antagonist. (C) Z48, an A<sub>2A</sub>-AR selective antagonist.

## 2. Materials and Methods

### 2.1. System Setup

The crystal structures of the two receptors were retrieved from PDB (the PDB code is 5N2S for A<sub>1</sub>-AR and 5NM4 for A<sub>2A</sub>-AR). Systems preparation was performed using a Molecular Operating Environment (MOE) suite (Chemical Computing Group ULC, Molecular Operating Environment (MOE), 2019.01. 1010 Sherbrooke St. West, Suite #910, Montreal, QC, Canada, H3A 2R7, 2019) [24] for protein preparation (removal of crystallographic water molecules, ions, and other solvent molecules, selection of the highest occupancy for each residue, assignment of the correct protonation state at pH 7.4). Systems preparation for the molecular dynamics simulations was carried out using VMD [25]. The protein was explicitly solvated in a water box with the borders placed at a distance of 15 Å from any protein atom, the water model used was TIP3P [26]. The system charge was neutralized to a concentration of 0.154 M using Na<sup>+</sup>/Cl<sup>-</sup>. The lipid bilayer consisted of phosphatidylcholine (POPC) units.

The sodium ion within the TMD allosteric site of A<sub>2A</sub>-AR was retained, and it was also placed by superposition in A<sub>1</sub>-AR.

### 2.2. Equilibration of the System

All the simulations were performed with a CHARMM36 force field [27] and using ACEMD2 [28]. Ligands parameters were retrieved from Paramchem [29], a web interface for the assignment of parameters based on the CGenFF [30] force field.

The system energy was minimized in 1500 steps using the conjugate-gradient method, then the equilibration of the system was done in four steps. The first one consisted of 5 ns of NPT simulation with harmonic positional constraints of 1 kcal mol<sup>-1</sup>Å<sup>-2</sup> on each atom of the protein and the lipid bilayer. The second step consisted in 10 ns of NPT simulation with harmonic positional constraints of 1 kcal mol<sup>-1</sup>Å<sup>-2</sup> only on each protein atom and on the phosphorus atom of the POPC units, the third step consisted in 5 ns of NPT simulation with harmonic positional constraints of 1 kcal mol<sup>-1</sup>Å<sup>-2</sup> only on the alpha carbons of the protein, and the last step consisted in 50 ns of NVT simulation without any constraints.

For the productive simulations, the temperature was maintained at 310 K using the Langevin thermostat, with a low dumping of 1 ps<sup>-1</sup>. The pressure was set at 1 atm using the Berendsen barostat [31]. The particle-mesh Ewald (PME) method was used to calculate the electrostatic interactions with a 1 Å grid [32]. A 9.0 Å cutoff was applied for long-term interactions. The M-SHAKE algorithm was applied to constrain the bond lengths involving hydrogen atoms.

At the end of the equilibration, several parameters were calculated to assess the stability of the system: the root mean square deviation (RMSD) of the alpha carbons of the protein, the root mean square fluctuation (RMSF) of each protein residue, the volume of the cell (which should tend to a plateau in the NPT ensemble), and the area per lipid (APL) for each membrane layer (calculated using GridMAT-MD [33]). We also computed the volume of the orthosteric site during the equilibration using POVME [34]. Figure S1 ( $A_{2A}$ -AR) and Figure S2 ( $A_1$ -AR) report the analysis performed during the equilibration of the system. In both the two systems, the protein reached a stable conformation (RMSD of the protein C $\alpha$  (panel A, Figures S1 and S2) stably below 2 Å for  $A_{2A}$ -AR and below 3 Å for  $A_1$ -AR). The volume of the orthosteric site reached a plateau in both cases (Panel B, Figures S1 and S2). The most flexible parts of the protein, as expected, are the loops. Indeed, the RMSF of these regions is higher than the TMs (panels C and D, Figures S1 and S2).

As shown in Figure S5, the orthosteric site of  $A_1$ -AR appears to be deeper than  $A_{2A}$ -AR, due to a cleft between TM5 and TM6. The APL and the volumetric analysis are reported in Figure S3 ( $A_1$ -AR) and Figure S4 ( $A_{2A}$ -AR). For both systems, the cell volume reached stable values.

### 2.3. Supervised Molecular Dynamics Simulations

SuMD [22,23] is a molecular dynamics (MD) approach that allows for the investigation of molecular recognition processes in a fully atomistic way, in the nanosecond timescale, without introducing any energetic bias (Figure 3). Ligands were placed 35 Å away from the protein. Each SuMD step was set to 600 ps. During each SuMD step, the distance between the center of mass of the binding site (defined by a series of residues) and the center of mass of the ligand is monitored. These data are then fitted, and if the slope of the interpolating linear function is negative, then the coordinates and the velocities are used for the successive time window, otherwise, the last time window is simulated again reassigning the velocities (this reassignment of the velocities is intrinsic in the use of Langevin thermostat). If the condition fails 30 consecutive times, then the simulation is stopped. Otherwise, the algorithm continues until the distance between the two centers of mass is below the threshold of 5 Å; at this point, the supervision is turned off and 30 short classical MD simulations are performed, switching on the supervision if the distance between the centroids becomes greater than 5 Å. At the end of the SuMD process, the trajectory is prolonged for 25 ns of classical MD simulation.

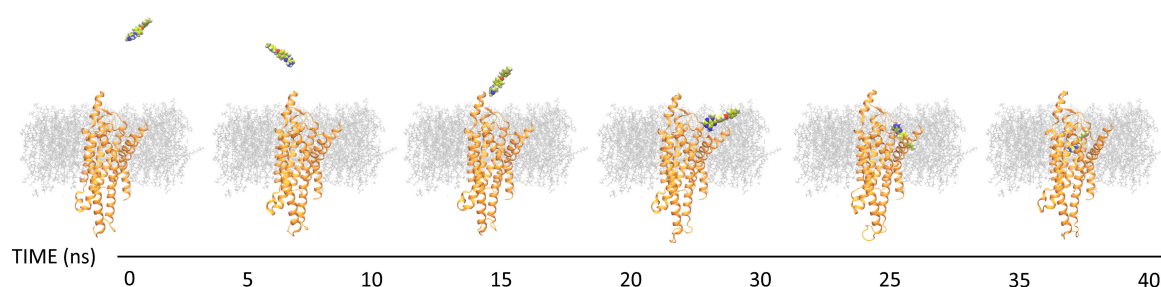


**Figure 3.** Representation of a binding event sampled by a supervised molecular dynamics (SuMD) simulation. After each reported step, the distance between the ligand and the binding site decreases. In less than (merged) 50 ns, a binding event was sampled.

Twenty simulations were performed for each of the six systems ( $Z48/A_1$ AR,  $Z48/A_{2A}$ AR,  $LC4/A_1$ AR,  $LC4/A_{2A}$ AR, Caffeine/ $A_1$ AR, Caffeine/ $A_{2A}$ AR). Only the simulations that sampled the ligand reaching the orthosteric site and interacting with the classic fingerprint of these class of ligands (Figure S6) were here reported (e.g., one replica for each system, excepted  $LC4/A_1$ AR for which two replicas were analyzed). For each system, the reasons for failure are similar. In most cases, the ligands interact strongly with the residues of the ECLs, and do not reach the binding site. In a few cases, the ligands only partially reach the orthosteric site. Finally, in other rare cases, the ligands get stuck between the protein and the membrane.

## 2.4. Trajectories Analysis

The SuMD trajectories were analyzed using an in-house python tool (described in [35]) that provides information on the geometry and the energetic of the system. The output consists of a per-residue analysis of the electrostatic and van Der Waals contributions to the protein-ligand interactions; a representation of the distance between the center of mass of the ligand and the center of mass of the binding site as a function of time; a global energetic evaluation of the system as a function of the aforementioned distance. This analysis allows comparing the energetic profile of two systems both in a general way and, through the per-residue analysis (i.e., it is possible to evaluate which ligand has better interaction with some specific amino acids of interest over the time).

Three replicas of 50 ns were performed on the apo form of A<sub>1</sub>-AR and A<sub>2A</sub>-AR, after the equilibration stage described before. These three replicas were merged and analyzed by AquaMMapS [36].

## 3. Results

### 3.1. SuMD Binding of the A<sub>1</sub>AR Nonselective Antagonist Caffeine

According to the SuMD simulations (Figures S7 and S8; Video S1 for A<sub>1</sub>AR and Video S2 for A<sub>2A</sub>AR in the Supplementary Information), the nonselective antagonist caffeine establishes intermediate interactions with the extracellular vestibule of A<sub>1</sub>AR and A<sub>2A</sub>AR, before reaching the orthosteric site. The most stable bound configurations sampled on A<sub>1</sub>AR and A<sub>2A</sub>AR differed for the orientation of the xanthine ring (Figure S9). On A<sub>2A</sub>AR, caffeine pointed the N7-methyl toward Asn253, while in A<sub>1</sub>AR it was rotated by 180°, with the N3 methyl in the proximity of Asn254. Notably, both these two conformations have been experimentally observed in X-ray crystal structures of A<sub>2A</sub>AR [17]. Fluctuations of the ligand in both orthosteric sites and the transient nature of the interactions are easily depicted in the energy interaction landscapes (Panels A, S7, S8) in which the points are particularly scattered over the distance between the centers of mass of the ligand and the orthosteric site.

### 3.2. SuMD Binding of the A<sub>2A</sub>AR Selective Antagonist Z48

Figures S10 and S11 report the analysis of Z48/A<sub>1</sub>AR and Z48/A<sub>2A</sub>AR, including 25 ns of classic MD simulations performed at the end of each SuMD simulation (Videos S3 and S4 in the Supplementary Information).

For what concerns the SuMD trajectory of Z48 on A<sub>1</sub>AR, notable electrostatic repulsion took place between the ligand and Lys168, Lys173, and Lys265, before the ligand reached the orthosteric site, as clearly observable in the per-residue electrostatic interaction energy plot (Panel C, S10). These residues are positioned on the ECLs (Lys168 and Lys173 on ECL2, and Lys265 on ECL3). As a result, in A<sub>1</sub>AR, Z48 did not adopt the binding fingerprint of the ARs antagonists (e.g., only one hydrogen bond with Asn254 out of two was formed). Moreover, this binding mode was unstable over the 25 ns of classic MD simulations. Interestingly, the terminal amine group of the ligand strongly interacts with Glu170 (Leu167 in A<sub>2A</sub>AR). Figure 4 reports the binding modes of Z48 at the end of the SuMD simulation on A<sub>1</sub>AR (the binding mode at the end of the 25 ns of classic MD simulation is shown in Figure S12) and A<sub>2A</sub>-AR (at the end of the 25 ns of classic MD simulation), respectively.

Moving to the binding simulations of Z48 to A<sub>2A</sub>AR, two SuMD replicas led to the classic binding mode of the ARs antagonists. The  $\pi$ - $\pi$  stacking with Phe168 was present, along with the hydrogen bonds with Asn253 and with Glu169. Both binding modes were stable during 25 ns of classic MD simulations (Figure S11, Panel C, D, Figure 4). No significant protein-ligand electrostatic repulsions were observed. The narrow funnel-like interaction energy profile of the ligand in the orthosteric also suggested a good complementarity of the ligand in the pocket, and a rapid reaching of a stable bound state.

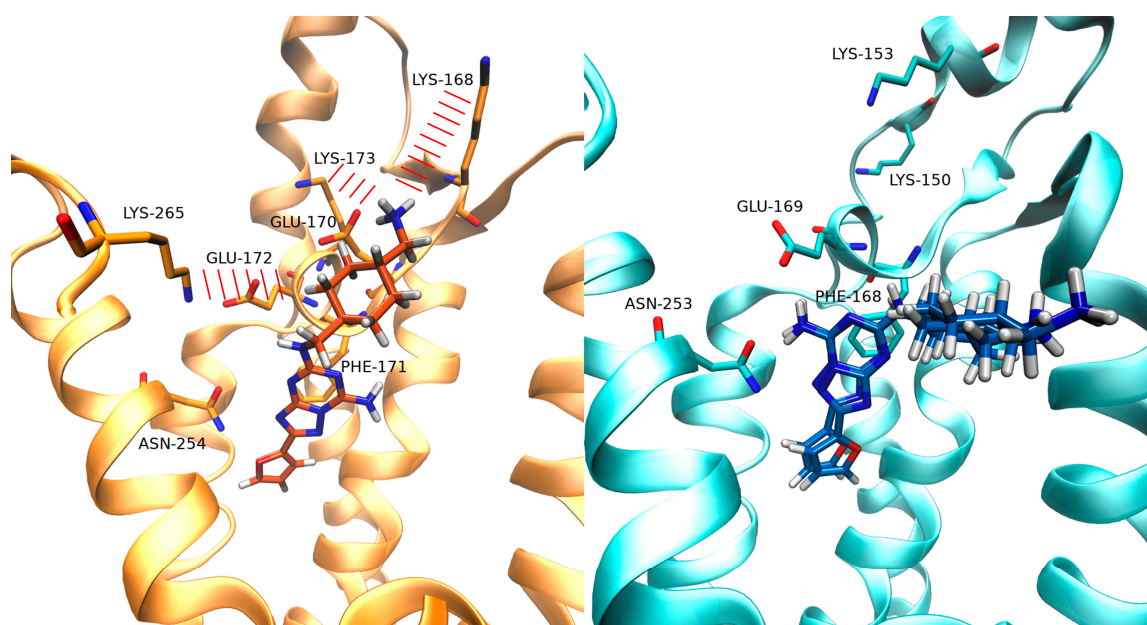


**Figure 4.** Binding mode of Z48 within the binding site of  $A_1$ -AR on the left-hand side, and within the binding site of  $A_{2A}$ -AR on the right-hand side (superposition of the two simulations analyzed). For  $A_1$ AR, the binding mode is reported at the end of the SuMD simulation. For  $A_{2A}$ AR, the two poses at the end of the classic MD simulation are reported.

### 3.3. SuMD Binding of the $A_1$ AR Selective Antagonist LC4

With regards to LC4, two SuMD replicas led to different binding modes of LC4 into the  $A_1$ AR orthosteric site. During Replica 1, the ligand formed a complex characterized by the xanthine scaffold positioned in the orthosteric binding site, and the N8-substituent pointed outward the receptor (Figure 5). A hydrogen bond with Asn254 and hydrophobic contacts with Phe171 occurred (Figure 6A). Interestingly, the LC4 oxygen atom in the N8 substituent interacted with and stabilized water molecules in the proximity of the Phe171 backbone, a hydrated spot on ECL3, according to the AquaMMaPS analysis (Figure 6A).

In the case of  $A_2$ AR, the xanthine scaffold reached the orthosteric site rotated by  $180^\circ$  compared to the binding mode adopted in  $A_1$ AR (Figure 6B) and with an unfavorable geometry for hydrogen bonding with Asn253. In both of these two binding modes (Figures S13 and S14), LC4 did not interact with conserved glutamate Glu172 ( $A_1$ AR) or Glu169 ( $A_{2A}$ AR).

During SuMD Replica 2 on  $A_1$ A, LC4 experienced a two-step binding (Figure 6). First, the antagonist entered the orthosteric site pointing the methylphenyl group into a hydrophobic pocket located between TM2 and TM3. This cryptic pocket is not present in  $A_2$ AR in light of bulkier residues and a higher degree of packing between the helices (Figure 6B). From this metastable configuration, LC4 moved deeper into the orthosteric site and engaged Asn254 and Glu172 in hydrogen bonds (Figure 6). In this binding mode, the ligand inserted the N8-substituent inside a further cryptic pocket between TM5 and TM6 (Figure 6C,D), which is delimited by the “toggle switch” residue W247 [15], and the residues Ile95 and Phe253, being part of the conserved class A structural motif PIF [37]. Notably, this hydrophobic sub-pocket was occupied by likely “unhappy” water molecules during simulations of the apo- $A_1$ R (Figure 6A).

The video of these three simulations can be found in Supplementary Materials Video S5 and Video S6 for the two simulations of LC4/ $A_1$ AR, and Video S7 for the simulation of LC4/ $A_{2A}$ AR.

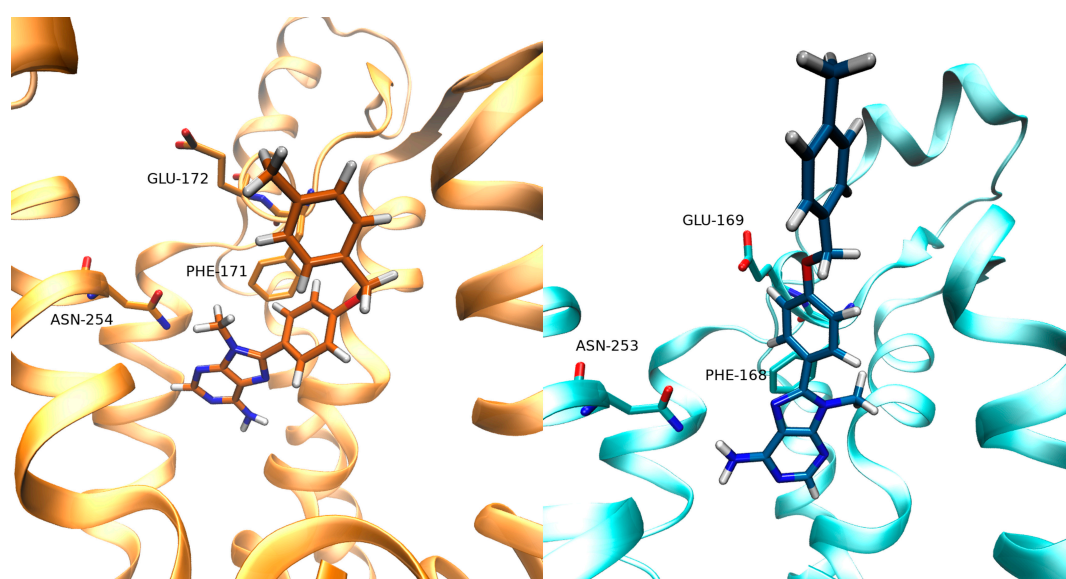


**Figure 5.** Binding mode of ligand LC4.  $A_1$ AR on the left and  $A_{2A}$ AR on the right.

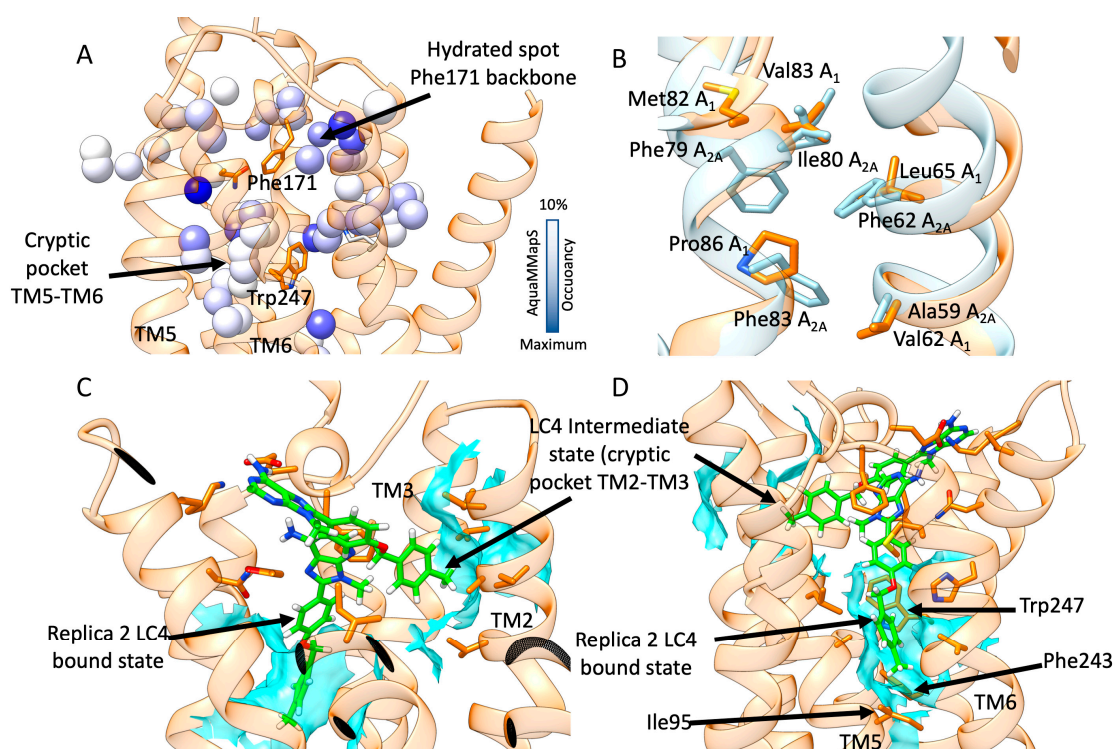


**Figure 6.** (A) Hydrated spots within  $A_1$ AR with AquaMMapSoccupancy > 10%. The cryptic pocket between TM5 and TM6, as well as the spot nearby the Phe171 backbone, are indicated; (B) comparison between  $A_1$ AR (orange) and  $A_{2A}$ AR (cyan) at the level of TM2 and TM3—a sub-pocket formed only in  $A_1$ AR during MD simulations, due to different residues and interhelical packing; (C) and (D) two side views of the two superimposed binding steps of LC4 (green stick) to  $A_1$ AR. Hydrophobic contacts are shown as cyan transparent surfaces.

#### 4. Discussion

Here we present results from SuMD simulations performed to shed light on the selectivity displayed by LC4 and Z48, two antagonists of  $A_1$ AR and  $A_{2A}$ AR, respectively. The nonselective antagonist caffeine was also dynamically docked to the two ARs subtype. Caffeine, which is in a weak

binder (micromolar range [38]) of all the ARs, experienced more than one binding mode, in line with our previous simulations [22] and experimental observation [17].

SuMD binding of the selective  $A_{2A}$ AR antagonist Z48 on  $A_1$ -AR and  $A_{2A}$ AR suggested different interaction patterns along the pathways. Z48 experienced unfavorable electrostatic interactions between positively charged  $A_1$ AR residues Lys168, Lys173 (ECL2), and Lys265 (ECL3), and the ligand charged amine on the N8-substituent. Such transitory states did not take place during binding to  $A_{2A}$ AR, as no significant electrostatic repulsions were computed at the extracellular vestibule. Interestingly,  $A_{2A}$ AR bears Ala265 instead of Lys265 on the ECL3, while Lys168 and Lys173 (ECL2) are farther from the binding site, compared to  $A_1$ AR. This is consistent with mutagenesis studies that demonstrated the importance of these lysine residues for the binding of several  $A_1$ AR ligands [39–41]. On  $A_{2A}$ AR, Z48 reached the orthosteric site producing the classic interactions fingerprint of the ARs antagonists. On  $A_1$ AR, on the other hand, the ligand sampled a different binding mode. Moreover, the  $A_1$ AR residue Glu170 (Val167 in  $A_{2A}$ AR) strongly interacted with the charged terminal amine of the ligand, stabilizing this alternative binding mode. Z48 was proposed to bind to  $A_2$ AR overcoming low enthalpy transition state(s) [40]. From this standpoint, the unfavorable electrostatic interactions with ECL2 could implicate a slower binding to  $A_1$ AR, and therefore a kinetic selectivity for  $A_2$ AR.

SuMD simulations of the antagonist LC4 proposed two possible binding modes that could drive selectivity. It is possible that the ligand binds  $A_1$ AR and  $A_{2A}$ AR with the same conformation, but differently interacting with water molecules nearby ECL3. From this standpoint, and in analogy with [41], we propose these “happy” water molecules contribute to the ligand stabilization in  $A_1$ AR (Figure S16), but not in  $A_2$ AR (Figure S17). An alternative and unique LC4 binding mechanism was sampled only on  $A_1$ AR, with a metastable state before the final complex formation. Along this pathway, two cryptic hydrophobic pockets (between TM2 and TM3 and between TM5 and TM6) allowed the N8-substituent of the ligand to correctly orient first, and then engage key residues for the receptor activation (the “toggle switch” Trp247, Ile95, and Phe253, which are part of the conserved class A motif PIF). Notably, the cryptic pocket between TM2 and TM3 has recently been proposed as a determinant for  $A_1$ AR selectivity displayed by the triazolotriazine antagonist LUF5452 [42,43].

## 5. Conclusions

Understanding the selectivity of GPCRs ligands is an important task in drug design. This study supports the emerging idea that selectivity is driven by a plethora of phenomena, other than the protein-ligand interactions in the bound state. Receptor-ligands recognitions are multistep events modulated by intermediate interaction along with the (un)binding paths. This picture may be further complicated by the presence of stable water molecules, which can have a tremendous impact on stabilizing or destabilizing an orthosteric complex. To consider different aspects that may affect the selectivity on  $A_1$ AR and  $A_{2A}$ AR, we used SuMD simulations to investigate the recognition of three different antagonists. Overall, our results suggest that kinetic selectivity may favor the binding of Z48 to  $A_{2A}$ AR over LC4. A different scenario was observed for  $A_1$ AR, the recognition trajectories highlighted the key role of water molecules in the binding mode of LC4, which is favored by two hidden sub pockets within  $A_1$ AR.

**Supplementary Materials:** The following are available online at <http://www.mdpi.com/2218-273X/10/5/732/s1>, Figure S1:  $A_{2A}$ AR, protein analysis during the equilibration stage, Figure S2:  $A_1$ AR, protein analysis during the equilibration stage. Figure S3:  $A_1$ AR system, cell volume analysis and membrane analysis. Figure S4:  $A_{2A}$ AR system, cell volume analysis and membrane analysis. Figure S5: Volumetric analysis (using POVME) of the orthosteric site of  $A_1$ AR and  $A_{2A}$ AR. Figure S6: X-Ray structure of  $A_{2A}$ AR in complex with caffeine and with ZMA. Figure S7: Analysis of the SuMD trajectory of binding for caffeine on  $A_1$ AR. Figure S8: Analysis of the SuMD trajectory of binding for caffeine on  $A_{2A}$ AR. Figure S9: Caffeine binding mode of caffeine within the binding site of  $A_1$ AR and  $A_{2A}$ AR. Figure S10: Analysis of the Z48 SuMD binding trajectory to  $A_1$ AR. Figure S11: Analysis of the SuMD trajectory of binding for Z48 on  $A_{2A}$ AR. Figure S12: Binding mode of Z48 in  $A_1$ AR at the end of the 25ns of classic MD. Figure S13 Analysis of the SuMD trajectory of binding for LC4 on  $A_1$ AR. Figure S14 Analysis of the SuMD trajectory of binding for LC4 on  $A_{2A}$ AR. Figure S15 Analysis of the SuMD trajectory of the alternative binding for LC4 on  $A_1$ AR. Figure S16: Interaction between LC4 and water molecules in  $A_1$ AR. Figure



S17: Interaction between LC4 and water molecules in A<sub>1</sub>AR and A<sub>2A</sub>AR. Video S1: Caffeine binding pathway against A<sub>1</sub>-AR., Video S2: Caffeine binding pathway against A<sub>2A</sub>-AR, Video S3: Z48 binding pathway against A<sub>1</sub>-AR. Video S4: Z48 binding pathway against A<sub>2A</sub>-AR. Video S5: LC4 binding pathway against A<sub>1</sub>-AR, binding mode 1. Video S6: LC4 binding pathway against A<sub>1</sub>-AR, binding mode 2. Video S7: LC4 binding pathway against A<sub>2A</sub>-AR.

**Author Contributions:** Conceptualization, S.M. and G.D.; methodology, G.D. and M.S.; software, G.D. and M.S.; validation, G.B., M.B. and G.D.; formal analysis, G.B.; investigation, G.B.; writing—original draft preparation, A.B.; writing—review and editing, G.D., M.B., M.S.; supervision, S.M.; project administration, S.M.; funding acquisition, S.M. All authors have read and agreed to the published version of the manuscript.

**Funding:** This research received no external funding.

**Acknowledgments:** MMS lab is very grateful to Chemical Computing Group, OpenEye, and Acellera for the scientific and technical partnership. MMS lab gratefully acknowledges the support of NVIDIA Corporation with the donation of the Titan V GPU used for this research.

**Conflicts of Interest:** The authors declare no conflict of interest.

## References

1. Müller, C.E.; Jacobson, K.A. Recent developments in adenosine receptor ligands and their potential as novel drugs. *Biochim. Biophys. Acta-Biomembr.* **2011**, *1808*, 1290–1308. [[CrossRef](#)] [[PubMed](#)]
2. Navarro, G.; Borroto-Escuela, D.O.; Fuxe, K.; Franco, R. Purinergic signaling in Parkinson's disease. Relevance for treatment. *Neuropharmacology* **2016**, *104*, 161–168. [[CrossRef](#)] [[PubMed](#)]
3. Gao, Z.G.; Jacobson, K.A. Purinergic signaling in mast cell degranulation and asthma. *Front. Pharmacol.* **2017**, *8*, 947. [[CrossRef](#)] [[PubMed](#)]
4. Chen, J.F.; Eltzschig, H.K.; Fredholm, B.B. Adenosine receptors as drug targets-what are the challenges? *Nat. Rev. Drug Discov.* **2013**, *12*, 265–286. [[CrossRef](#)]
5. Moro, S.; Gao, Z.G.; Jacobson, K.A.; Spalluto, G. Progress in the pursuit of therapeutic adenosine receptor antagonists. *Med. Res. Rev.* **2006**, *26*, 131–159. [[CrossRef](#)]
6. Shah, U.; Hodgson, R. Recent progress in the discovery of adenosine A<sub>2A</sub> receptor antagonists for the treatment of Parkinson's disease. *Curr. Opin. Drug Discov. Dev.* **2010**, *13*, 466–480.
7. Kiesman, W.F.; Elzein, E.; Zablocki, J. A<sub>1</sub> adenosine receptor antagonists, agonists, and allosteric enhancers. *Handb. Exp. Pharmacol.* **2009**, *193*, 25–58.
8. Cristalli, G.; Müller, C.E.; Volpini, R. Recent developments in Adenosine A<sub>2A</sub> receptor ligands. *Handb. Exp. Pharmacol.* **2009**, *193*, 59–98.
9. Manera, C.; Saccomanni, G. A<sub>2A</sub> receptor ligands: Past, present and future trends. *Curr. Top. Med. Chem.* **2010**, *10*, 902–922. [[CrossRef](#)]
10. Baraldi, P.G.; Tabrizi, M.A.; Fruttarolo, F.; Romagnoli, R.; Preti, D. Recent improvements in the development of A<sub>2B</sub> adenosine receptor agonists. *Purinergic Signal.* **2009**, *5*, 3–19. [[CrossRef](#)]
11. Ortore, G.; Martinelli, A. A<sub>2B</sub> receptor ligands: Past, present and future trends. *Curr. Top. Med. Chem.* **2010**, *10*, 923–940. [[CrossRef](#)] [[PubMed](#)]
12. Jacobson, K.A.; Klutz, A.M.; Tosh, D.K.; Ivanov, A.A.; Preti, D.; Baraldi, P.G. Medicinal chemistry of the A<sub>3</sub> adenosine receptor: Agonists, antagonists, and receptor engineering. *Handb. Exp. Pharmacol.* **2009**, *193*, 123–159.
13. Müller, C.E.; Jacobson, K.A. Xanthines as adenosine receptor antagonists. *Handb. Exp. Pharmacol.* **2011**, *200*, 151–199.
14. Schenone, S.; Brullo, C.; Musumeci, F.; Bruno, O.; Botta, M. A<sub>1</sub> receptors ligands: Past, present and future trends. *Curr. Top. Med. Chem.* **2010**, *10*, 878–901. [[CrossRef](#)] [[PubMed](#)]
15. Jespers, W.; Schiedel, A.C.; Heitman, L.H.; Cooke, R.M.; Kleene, L.; van Westen, G.J.P.; Gloriam, D.E.; Müller, C.E.; Sotelo, E.; Gutiérrez-de-Terán, H. Structural mapping of adenosine receptor mutations: ligand binding and signaling mechanisms. *Trends Pharmacol. Sci.* **2018**, *39*, 75–89. [[CrossRef](#)]
16. Glukhova, A.; Thal, D.M.; Nguyen, A.T.; Vecchio, E.A.; Jörg, M.; Scammells, P.J.; May, L.T.; Sexton, P.M.; Christopoulos, A. Structure of the adenosine A<sub>1</sub> receptor reveals the basis for subtype selectivity. *Cell* **2017**, *168*, 867–877. [[CrossRef](#)]

17. Cheng, R.K.Y.; Segala, E.; Robertson, N.; Deflorian, F.; Doré, A.S.; Errey, J.C.; Fiez-Vandal, C.; Marshall, F.H.; Cooke, R.M. Structures of human A1 and A2A Adenosine receptors with xanthines reveal determinants of selectivity. *Structure* **2017**, *25*, 1275–1285. [CrossRef]
18. Draper-Joyce, C.J.; Khoshouei, M.; Thal, D.M.; Liang, Y.L.; Nguyen, A.T.N.; Furness, S.G.B.; Venugopal, H.; Baltos, J.A.; Plitzko, J.M.; Danev, R.; et al. Structure of the adenosine-bound human adenosine A1 receptor-Gi complex. *Nature* **2018**, *558*, 559–563. [CrossRef]
19. Sykes, D.A.; Stoddart, L.A.; Kilpatrick, L.E.; Hill, S.J. Binding kinetics of ligands acting at GPCRs. *Mol. Cell. Endocrinol.* **2019**, *485*, 9–19. [CrossRef]
20. Federico, S.; Paoletta, S.; Cheong, S.L.; Pastorin, G.; Cacciari, B.; Stragliotto, S.; Norbert Klotz, K.; Siegel, J.; Gao, Z.G.; Jacobson, K.A.; et al. Synthesis and biological evaluation of a new series of 1, 2, 4-triazolo[1, 5- $\alpha$ ]-1, 3, 5-triazines as human a2a adenosine receptor antagonists with improved water solubility. *J. Med. Chem.* **2011**, *54*, 877–889. [CrossRef]
21. Lambertucci, C.; Buccioni, M.; Cacciari, B.; Dal Ben, D.; Federico, S.; Klotz, K.N.; Marucci, G.; Volpini, R.; Spalluto, G.; Cristalli, G. New 9-methyl-8-(4-hydroxyphenyl)adenine derivatives as A1 adenosine receptor antagonists. *Collect. Czechoslov. Chem. Commun.* **2011**, *76*, 1379–1393. [CrossRef]
22. Sabbadin, D.; Moro, S. Supervised molecular dynamics (SuMD) as a helpful tool to depict GPCR-ligand recognition pathway in a nanosecond time scale. *J. Chem. Inf. Model.* **2014**, *54*, 372–376. [CrossRef] [PubMed]
23. Cuzzolin, A.; Sturlese, M.; Deganutti, G.; Salmaso, V.; Sabbadin, D.; Ciancetta, A.; Moro, S. Deciphering the complexity of ligand-protein recognition pathways using supervised molecular dynamics (SuMD) simulations. *J. Chem. Inf. Model.* **2016**, *56*, 687–705. [CrossRef] [PubMed]
24. Chemical Computing Group ULC. *Molecular Operating Environment (MOE)*; CCG: Montreal, QC, Canada, 2019.
25. Humphrey, W.; Dalke, A.; Schulten, K. VMD: Visual molecular dynamics. *J. Mol. Graph.* **1996**, *14*, 33–38. [CrossRef]
26. Jorgensen, W.L.; Chandrasekhar, J.; Madura, J.D.; Impey, R.W.; Klein, M.L. Comparison of simple potential functions for simulating liquid water. *J. Chem. Phys.* **1983**, *79*, 926–935. [CrossRef]
27. Brooks, B.R.; Brooks, C.L.; Mackerell, A.D.; Nilsson, L.; Petrella, R.J.; Roux, B.; Won, Y.; Archontis, G.; Bartels, C.; Boresch, S.; et al. CHARMM: The biomolecular simulation program. *J. Comput. Chem.* **2009**, *30*, 1545–1614. [CrossRef] [PubMed]
28. Harvey, M.J.; Giupponi, G.; Fabritiis, G. De ACEMD: Accelerating Biomolecular dynamics in the microsecond time scale. *J. Chem. Theory Comput.* **2009**, *5*, 1632–1639. [CrossRef]
29. Available online: <https://cgenff.umaryland.edu/> (accessed on 29 April 2020).
30. Vanommeslaeghe, K.; Hatcher, E.; Acharya, C.; Kundu, S.; Zhong, S.; Shim, J.; Darian, E.; Guvench, O.; Lopes, P.; Vorobyov, I.; et al. CHARMM general force field: A force field for drug-like molecules compatible with the CHARMM all-atom additive biological force fields. *J. Comput. Chem.* **2010**, *31*, 671–690. [CrossRef]
31. Berendsen, H.J.C.; Postma, J.P.M.; van Gunsteren, W.F.; DiNola, A.; Haak, J.R. Molecular dynamics with coupling to an external bath. *J. Chem. Phys.* **1984**, *81*, 3684–3690. [CrossRef]
32. Essmann, U.; Perera, L.; Berkowitz, M.L.; Darden, T.; Lee, H.; Pedersen, L.G. A smooth particle mesh Ewald method. *J. Chem. Phys.* **1995**, *103*, 8577–8593. [CrossRef]
33. Allen, W.J.; Lemkul, J.A.; Bevan, D.R. GridMAT-MD: A grid-based membrane analysis tool for use with molecular dynamics. *J. Comput. Chem.* **2009**, *30*, 1952–1958. [CrossRef] [PubMed]
34. Wagner, J.R.; Sørensen, J.; Hensley, N.; Wong, C.; Zhu, C.; Perison, T.; Amaro, R.E. POVME 3.0: Software for Mapping Binding Pocket Flexibility. *J. Chem. Theory Comput.* **2017**, *13*, 4584–4592. [CrossRef] [PubMed]
35. Salmaso, V.; Sturlese, M.; Cuzzolin, A.; Moro, S. Exploring protein-peptide recognition pathways using a supervised molecular dynamics approach. *Structure* **2017**, *25*, 655–662. [CrossRef] [PubMed]
36. Cuzzolin, A.; Deganutti, G.; Salmaso, V.; Sturlese, M.; Moro, S. AquaMMapS: An alternative tool to monitor the role of water molecules during protein-ligand association. *ChemMedChem* **2018**, *13*, 522–531. [CrossRef] [PubMed]
37. Wacker, D.; Wang, C.; Katritch, V.; Han, G.W.; Huang, X.P.; Vardy, E.; McCorvy, J.D.; Jiang, Y.; Chu, M.; Siu, F.Y.; et al. Structural features for functional selectivity at serotonin receptors. *Science* **2013**, *340*, 615–619. [CrossRef] [PubMed]
38. Ishiyama, H.; Ohshita, K.; Abe, T.; Nakata, H.; Kobayashi, J. Synthesis of eudistomin D analogues and its effects on adenosine receptors. *Bioorganic Med. Chem.* **2008**, *16*, 3825–3830. [CrossRef]

39. Nguyen, A.T.N.; Baltos, J.A.; Thomas, T.; Nguyen, T.D.; Muñoz, L.L.; Gregory, K.J.; White, P.J.; Sexton, P.M.; Christopoulos, A.; May, L.T. Extracellular loop 2 of the adenosine A1 receptor has a key role in orthosteric ligand affinity and agonist efficacy. *Mol. Pharmacol.* **2016**, *90*, 703–714. [[CrossRef](#)]
40. Dawson, E.S.; Wells, J.N. Determination of amino acid residues that are accessible from the ligand binding crevice in the seventh transmembrane-spanning region of the human A1 adenosine receptor. *Mol. Pharmacol.* **2001**, *59*, 1187–1195. [[CrossRef](#)]
41. Deganutti, G.; Zhukov, A.; Deflorian, F.; Federico, S.; Spalluto, G.; Cooke, R.M.; Moro, S.; Mason, J.S.; Bortolato, A. Impact of protein–ligand solvation and desolvation on transition state thermodynamic properties of adenosine A2A ligand binding kinetics. *Silico Pharmacol.* **2017**, *5*, 16. [[CrossRef](#)]
42. Bortolato, A.; Tehan, B.G.; Bodnarchuk, M.S.; Essex, J.W.; Mason, J.S. Water network perturbation in ligand binding: Adenosine A2A antagonists as a case study. *J. Chem. Inf. Model.* **2013**, *53*, 1700–1713. [[CrossRef](#)]
43. Mattedi, G.; Deflorian, F.; Mason, J.S.; De Graaf, C.; Gervasio, F.L. Understanding ligand binding selectivity in a prototypical GPCR family. *J. Chem. Inf. Model.* **2019**, *59*, 2830–2836. [[CrossRef](#)] [[PubMed](#)]



© 2020 by the authors. Licensee MDPI, Basel, Switzerland. This article is an open access article distributed under the terms and conditions of the Creative Commons Attribution (CC BY) license (<http://creativecommons.org/licenses/by/4.0/>).